

## Energy-Efficient Electrosynthesis of High Value-Added Active Chlorine Coupled with H<sub>2</sub> Generation from Direct Seawater Electrolysis through Decoupling Electrolytes

Angewandte Chemie-International Edition

Zhu, Wenxin; Wei, Ziyi; Ma, Yiyue; Ren, Meirong; Fu, Xue et al

<https://doi.org/10.1002/anie.202319798>

This publication is made publicly available in the institutional repository of Wageningen University and Research, under the terms of article 25fa of the Dutch Copyright Act, also known as the Amendment Taverne.

Article 25fa states that the author of a short scientific work funded either wholly or partially by Dutch public funds is entitled to make that work publicly available for no consideration following a reasonable period of time after the work was first published, provided that clear reference is made to the source of the first publication of the work.

This publication is distributed using the principles as determined in the Association of Universities in the Netherlands (VSNU) 'Article 25fa implementation' project. According to these principles research outputs of researchers employed by Dutch Universities that comply with the legal requirements of Article 25fa of the Dutch Copyright Act are distributed online and free of cost or other barriers in institutional repositories. Research outputs are distributed six months after their first online publication in the original published version and with proper attribution to the source of the original publication.

You are permitted to download and use the publication for personal purposes. All rights remain with the author(s) and / or copyright owner(s) of this work. Any use of the publication or parts of it other than authorised under article 25fa of the Dutch Copyright act is prohibited. Wageningen University & Research and the author(s) of this publication shall not be held responsible or liable for any damages resulting from your (re)use of this publication.

For questions regarding the public availability of this publication please contact [openaccess.library@wur.nl](mailto:openaccess.library@wur.nl)

# Energy-Efficient Electrosynthesis of High Value-Added Active Chlorine Coupled with H<sub>2</sub> Generation from Direct Seawater Electrolysis through Decoupling Electrolytes

Wenxin Zhu, Ziyi Wei, Yiyue Ma, Meirong Ren, Xue Fu, Min Li, Chunling Zhang, Jianlong Wang,\* and Shaojun Guo\*

**Abstract:** Direct saline (seawater) electrolysis is a well-recognized system to generate active chlorine species for the chloride-mediated electrosynthesis, environmental remediation and sterilization over the past few decades. However, the large energy consumption originated from the high cell voltage of traditional direct saline electrolysis system, greatly restricts its practical application. Here, we report an acid-saline hybrid electrolysis system for energy-saving co-electrosynthesis of active chlorine and H<sub>2</sub>. We demonstrate that this system just requires a low cell voltage of 1.59 V to attain 10 mA cm<sup>-2</sup> with a large energy consumption decrease of 27.7% compared to direct saline electrolysis system (2.20 V). We further demonstrate that such acid-saline hybrid electrolysis system could be extended to realize energy-saving and sustainable seawater electrolysis. The acidified seawater in this system can absolutely avoid the formation of Ca/Mg-based sediments that always form in the seawater electrolysis system. We also prove that this system in the half-flow mode can realize real-time preparation of active chlorine used for sterilization and pea sprout production.

which commonly includes the chlorine evolution reaction (CER) and other two kinds of COR for active chlorine (AC) formation.<sup>[1,2]</sup> The occurrence of these reactions mainly depends on the electrolyte, applied potential, Cl<sup>-</sup> concentration and temperature. Based on the Pourbaix diagram for aqueous chloride chemistry,<sup>[1,3]</sup> in low concentration of neutral saline or natural seawater, the COR for the formation of AC like hypochlorous acid (HClO) and hypochlorite (ClO<sup>-</sup>) dominates over CER.<sup>[1,2]</sup> Meanwhile, in the whole pH range, although oxygen evolution reaction (OER) is thermodynamically preferred over COR, the COR with rapid two-electron transfer kinetics has a high possibility to occur earlier than OER in acidic, neutral and even weakly alkaline saline with much increased currents (with suitable Cl<sup>-</sup> concentration and catalyst).<sup>[4,5]</sup> Besides, the HClO, ClO<sup>-</sup> and Cl radical generated in COR process in SE system have already been applied in chloride-mediated electrosynthesis,<sup>[6-9,10]</sup> environmental remediation,<sup>[11-13]</sup> and inactivation of bacteria and viruses like SARS-CoV-2.<sup>[14-16]</sup> Considering the advantageous condition of COR occurrence and high value of AC, COR electrocatalysts as well as COR-mediated electrolysis systems especially the SE system have received increasing attention.<sup>[1,2,17,18]</sup>

Nevertheless, from the Pourbaix diagrams for aqueous chloride and water, we can quantitatively observe that the thermodynamic equilibrium potential ( $E_0$ ) of COR is still as high as ~1.28 V (vs. SHE) in neutral saline with low concentration, ~464 mV higher than that for OER ( $E_0$  in neutral saline; 0.816 V vs. SHE) and also much higher than those for many other organic/inorganic molecule oxidation reactions. The  $E_0$  difference between COR and OER will be enlarged to ~480 mV in seawater (pH of ~8.0),<sup>[1,3]</sup> and in fact, this difference in neutral saline will also be stabilized at this value after electrolysis for some time. Meanwhile, in the SE system, the cathodic hydrogen evolution reaction (HER) is also thermodynamically unfavorable compared to that occurred in acid ( $E_0$  in neutral saline; -0.414 V vs. SHE), and always has a slow kinetics due to the high solution resistance and low H<sup>+</sup>/OH<sup>-</sup> concentrations of saline.<sup>[19]</sup> These unfavorable factors result in a high energy consumption (cell voltage far exceeds the theoretical value of 1.694 V) of the SE system. Therefore, how to reduce the energy consumption of this system to generate AC and green H<sub>2</sub> should be concerned. Although the overpotential of acidic/saline CER/COR could be reduced to very low values of tens of millivolts via rational design of advanced

## Introduction

In the industrial chlor-alkali and saline/seawater electrolysis (SE) systems, chloride electro-oxidation reaction (COR) is a very important and complicated process occurred at anode,

[\*] Prof. W. Zhu, Z. Wei, Y. Ma, X. Fu, M. Li, Prof. C. Zhang,

Prof. J. Wang

College of Food Science and Engineering

Northwest A&F University

Yangling 712100, Shaanxi, China

E-mail: wanglong79@nwsuaf.edu.cn

Prof. S. Guo

School of Materials Science & Engineering

Peking University

Beijing 100871, China

E-mail: guosj@pku.edu.cn

M. Ren

Department of Agrotechnology and Food Sciences

Wageningen University & Research

Droevendaalsesteeg 2, 6708 PB Wageningen, The Netherlands

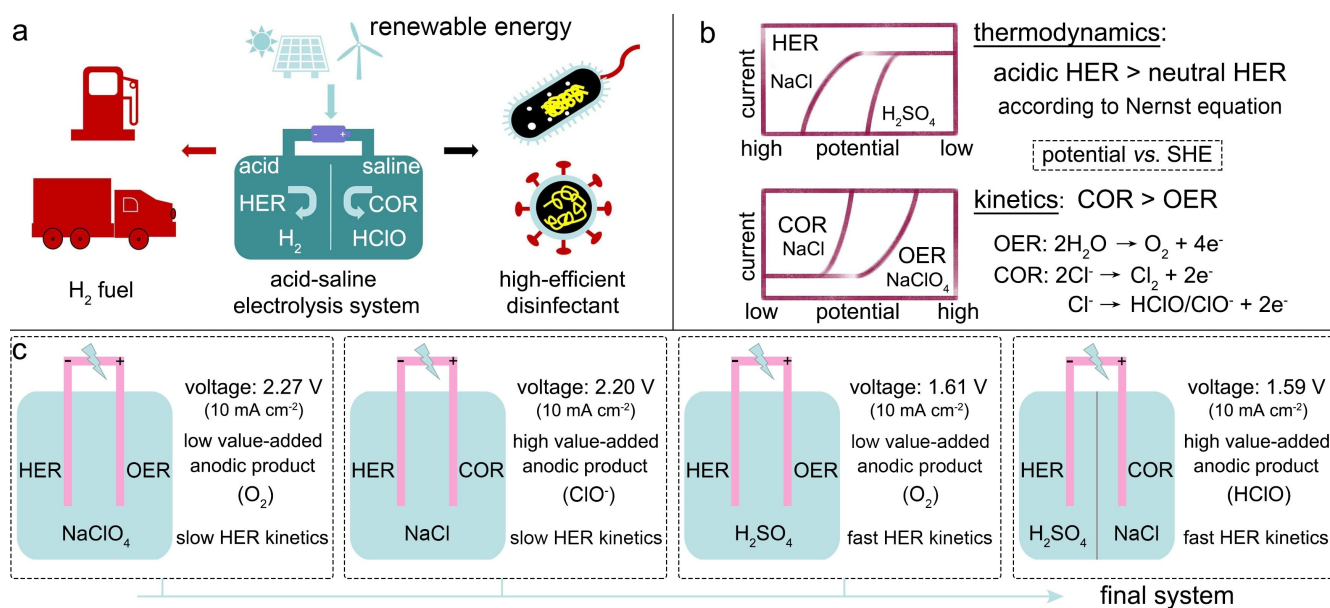
catalysts,<sup>[4,11,20–25]</sup> the decrease of cell voltage of SE system is still quite limited, mainly due to the relative-high overpotential of saline HER (compared to HER in acid, base and even phosphate buffered solution) caused by its extra water dissociation process and intrinsic high  $E_0$  as well as the relative low conductivity of saline. Aside from the concern of energy consumption, it should also be noted that the AC generated in the SE system is mainly  $\text{ClO}^-$ , the oxidation activity of which is indeed much lower than  $\text{HClO}$ .<sup>[26]</sup> Meanwhile, although the diaphragm SE system could produce  $\text{HClO}$ , high cell voltage far beyond theoretical 1.694 V is still always needed. In addition, in SE system (without diaphragm), the electrolyte pH will rise with the prolonging of electrolysis time. Therefore, the COR will be inhibited by OER, and  $\text{Ca}^{2+}/\text{Mg}^{2+}$  existed in natural seawater will react with  $\text{OH}^-$  in alkalized seawater during electrolysis to form sediments that will poison catalysts and degrade their catalytic activity and durability.<sup>[1–3,27,28]</sup> Furthermore, the mixture of  $\text{H}_2$  and chlorine generated in this system is unsafe and subsequent separation procedure is essential. These above problems in the SE system, however, have not been solved well.

Herein, we report a proof-of-concept demonstration that coupling acidic HER with saline COR could realize simultaneous production of AC disinfectant and  $\text{H}_2$  with low energy consumption (Scheme 1a). In addition to the two main theoretical basis of the lower thermodynamic potential of acidic HER over saline HER and faster kinetics of saline COR over saline OER (Scheme 1b), it is worth noting that the acidified anolyte during COR process in this system will further reduce the  $E_0$  difference of OER and COR,<sup>[1,5]</sup> and avoid the formation of  $\text{Ca}/\text{Mg}$ -based sediments that always form in seawater electrolysis system. A comprehensive comparison of different electrolysis systems in other aspects is shown in Scheme 1c and Figure S1. In this work, the ASE

and seawater-included ASE systems were successfully fabricated to realize energy-saving co-electrosynthesis of  $\text{HClO}$  and  $\text{H}_2$ . The ASE system in a half-flow mode was then built in order to prepare  $\text{HClO}$  in real time. The high inactivation efficiencies of the prepared  $\text{HClO}$  toward *Escherichia coli* (*E. coli*) and *Staphylococcus aureus* (*S. aureus*) were then demonstrated. Meanwhile, the produced  $\text{HClO}$  was also preliminarily found capable of controlling the surface coliform number and promoting the growth of pea sprouts to a certain extent.

## Results and Discussion

To experimentally evaluate the feasibility of the ASE system, a monolithic TiRu/Ti electrode with desired high and stable catalytic activities toward neutral/acidic HER, OER and COR was prepared. The synthetic process (Figure S2) includes hydrothermal deposition of TiRu-precursor on Ti mesh and annealing conversion of it into TiRu nanorod array. The X-ray diffraction pattern (Figure S3) of TiRu/Ti indicates that the surface TiRu species are composed of  $\text{TiO}_2$  and Ru phases. The scanning electron microscopy images in Figure S4a and S4b show that the skeleton of Ti mesh is totally covered with tightly grown TiRu nanorod array. The energy-dispersive X-ray spectrum and elemental mapping images (Figure S5) provide the information of elemental composition and distribution in TiRu nanoarray. The transmission electron microscopy (TEM) and high-resolution TEM images (Figure S6) illustrate that single TiRu nanorod has a rough surface and crystalline structure with the lattice spacings of 0.238 and 0.333 nm that correspond well to the (100) and (110) planes of Ru and  $\text{TiO}_2$ , respectively.



**Scheme 1.** Schematic illustration and design principle of the ASE system based on TiRu/Ti. (a) Schematic illustration. (b) Two main theoretical basis of system design. (c) Comparison of different electrolysis systems in other aspects except the two points referred in b.

X-ray photoelectron spectroscopy was applied to investigate the surface chemical composition and elemental valence states in the TiRu nanoarray. Figure S7a shows the deconvoluted Ru 3d core-level XPS spectrum. Due to the Ru 3d<sub>3/2</sub> located at ~284.4 eV is overlapped with C 1s signal, the composition of Ru species was only investigated by the Ru 3d<sub>5/2</sub> signal. The peak located at ~280.3 eV could be ascribed to Ru<sup>0</sup>.<sup>[29]</sup> Meanwhile, as presented in the Ru 3p and Ti 2p core-level spectrum (Figure S7b), the Ru 3p<sub>3/2</sub> and Ru 3p<sub>1/2</sub> peaks, located respectively at 462.3 and 485.0 eV, could also be attributed to the Ru<sup>0</sup> for metallic Ru.<sup>[30,31]</sup> The peaks at 464.5 and 458.8 eV with the spin-orbit splitting of 5.7 eV are assigned to typical Ti 2p<sub>1/2</sub> and Ti 2p<sub>3/2</sub> in TiO<sub>2</sub>, respectively.<sup>[32]</sup> The O 1s spectrum (Figure S7c) includes two characteristic peaks: one peak at 530.1 eV attributed to the lattice oxygen and another broad peak at near 532 eV referred to the oxygen vacancy and surface chemisorbed oxygen.<sup>[33,34]</sup>

The COR, HER and overall electrolysis performances in saline of TiRu/Ti were evaluated. As can be seen in Figure 1a, the HER performance of TiRu/Ti in 1.0 M NaCl is similar with the one in 1.0 M NaClO<sub>4</sub>. Both of them show high HER activity in saline. Figure 1b shows that the COR reaction in NaCl on the TiRu/Ti electrode occurs at a lower

onset-potential, and has a higher current response than OER in NaClO<sub>4</sub>, indicating that the COR will occur indeed earlier than OER on the surface of TiRu/Ti with a suitable Cl<sup>-</sup> concentration. The COR performance of TiRu/Ti is also higher than that of RuO<sub>2</sub>/Ti. Besides, the Faradaic efficiency of this electrode toward COR was calculated to be ~83.3% based on a standard iodometric titration method,<sup>[11,21]</sup> indicative of a high COR selectivity of TiRu/Ti in NaCl. The LSV curves with *iR* correction (Figure S8a and S9a) and derived Tafel slopes (Figure S8b and S9b) of different electrodes toward neutral HER and saline COR further prove the high activities and rapid reaction kinetics of TiRu/Ti toward half reactions.<sup>[35]</sup> Besides, the long-term chrono-potentiometry (CP) and multi-step CP curves (Figure 1c, Figure S10 and S11) demonstrate the satisfactory mechanical robustness and stability of TiRu/Ti toward saline HER and COR.

Figure 1d shows the schematic diagram of direct SE system (NaCl-NaCl) for the production of ClO<sup>-</sup>. Figure 1e records the overall electrolysis performances of different electrode pairs in 1.0 M NaCl and TiRu/Ti (+, -) in 1.0 M NaClO<sub>4</sub>. The results show that TiRu/Ti (+, -) needs a relatively low cell voltage of ~2.20 V to afford a current density of 10 mA cm<sup>-2</sup> in NaCl, not only over 70 mV lower

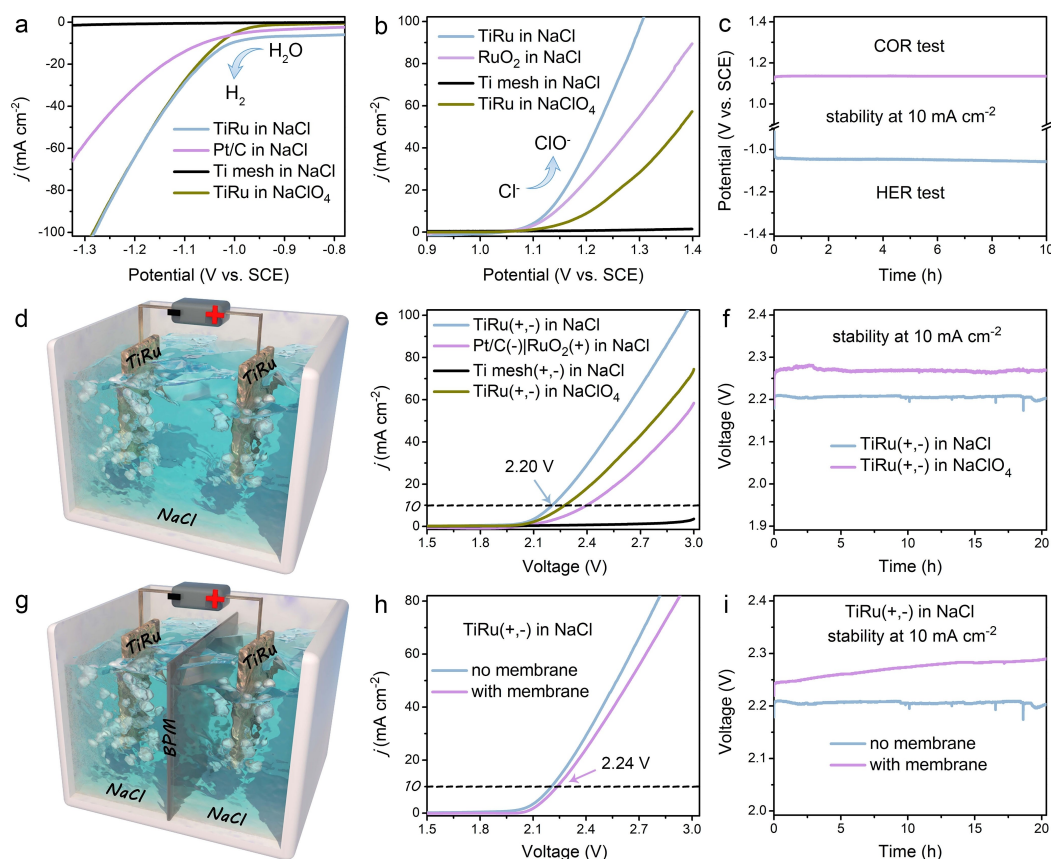


**Figure 1.** Performance evaluation of the SE system driven by TiRu/Ti. (a) HER curves of different electrodes in 1.0 M NaCl and TiRu/Ti in 1.0 M NaClO<sub>4</sub>. (b) LSV curves of different electrodes in NaCl for COR and TiRu/Ti in NaClO<sub>4</sub> for OER. (c) CP curves at  $|10|$  mA cm<sup>-2</sup> of TiRu/Ti toward HER and COR in NaCl. (d) Schematic diagram of the SE system. (e) System performances of different electrode pairs in NaCl and TiRu/Ti (+, -) in NaClO<sub>4</sub>. (f) CP curves of TiRu/Ti (+, -) toward overall electrolysis in NaCl and NaClO<sub>4</sub>. (g) Schematic diagram of the diaphragm SE system. (h) Performance and (i) long-term stability curves of SE systems with and without diaphragm.

than that for TiRu/Ti (+, -) in NaClO<sub>4</sub>, but also much lower than that for Pt/C-RuO<sub>2</sub> pair in NaCl. This result indicates that the introduction of anodic alternative COR with faster reaction kinetics instead of OER could indeed reduce the required voltage for H<sub>2</sub> production. The long-term CP curves (Figure 1f) indicate that TiRu/Ti (+, -) could catalyze durably both the neutral water splitting and NaCl electrolysis. Moreover, the diaphragm SE system (NaCl||NaCl) was fabricated (Figure 1g), which is the simplified SE model to produce HClO. Figure 1h shows the performances of SE systems with and without diaphragm. Obviously, the performance of diaphragm SE system is a little worse than that for SE system due to the extra membrane resistance. In addition, different from SE system, the operational stability of diaphragm SE system is poor (Figure 1i), which is mainly due to the pH variation of electrolyte in long-term test.

Moreover, according to the Pourbaix diagram of water (Figure 2a), we can see that the  $E_0$  value of acidic HER is much lower than that of neutral HER, while the  $E_0$  value of neutral OER is also much lower than that of acidic OER. Meanwhile, the suitable high-efficiency catalysts could improve the kinetics of specific reactions, and various electrolytes (like H<sub>2</sub>SO<sub>4</sub>, KOH, NaCl) with different solution resistances ( $R_s$ ) could also lead to the difference of reaction kinetics, both of which have impact on the overpotential and

increase rate of current vs. potential in actual polarization curves. Figure 2b shows the acidic and neutral HER LSV curves of TiRu/Ti without  $iR$  correction. Obviously, the potentials at different currents for acidic HER are over 600 mV lower than those for neutral HER, dominated by the difference of  $E_0$  (affected by pH effect) and  $R_s$ . The Faradaic efficiency of TiRu/Ti toward acidic HER was tested by drainage method and calculated to be ~97% (Figure S12). Meanwhile, the recorded multi-step (Figure S13a) and long-term (Figure S13b) CP curves also indicate that the TiRu/Ti has a robust HER performance in acid.

Besides, as can be seen from the acidic and neutral OER as well as neutral COR curves in Figure 2c (without  $iR$  correction), although COR itself has a higher  $E_0$  compared with neutral OER, neutral COR occurs however at a lower onset-potential with faster current increase, ascribed to the faster reaction kinetics of COR against OER and high COR selectivity of the TiRu/Ti. Although neutral OER occurs at a relative lower potential than acidic OER, its current increase is slower than that for acidic OER mainly due to the large  $R_s$  of NaCl. As mentioned above, the differences reflected on the potential and current in LSV curves are caused by the combined influences of  $E_0$  and intrinsic kinetics of half reactions, catalyst and  $R_s$ .

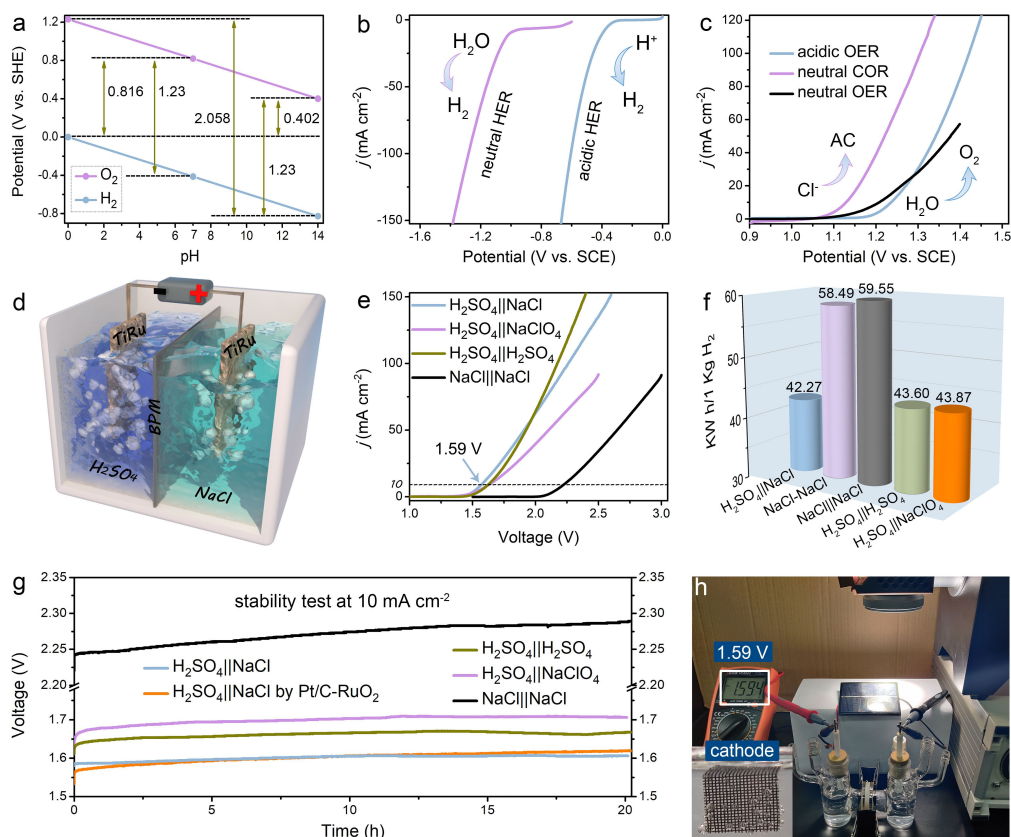


**Figure 2.** Performance evaluation of the ASE system driven by TiRu/Ti. (a) Pourbaix diagram of water calculated by the Nernst equation. (b) Neutral (1.0 M NaCl) and acidic (0.5 M H<sub>2</sub>SO<sub>4</sub>) HER curves. (c) Neutral/acidic OER and neutral COR curves. (d) Schematic diagram of the ASE system. (e) Performance curves and (f) required quantities of electricity to obtain 1.0 kg H<sub>2</sub> of different electrolysis systems. (g) Long-term stability curves of different electrolysis systems driven by TiRu/Ti and ASE system driven by Pt/C-RuO<sub>2</sub>. (h) Photograph of simulated sunlight-driven ASE system.

We then coupled acidic HER with saline COR reactions in one electrolysis system for realizing energy-saving production of  $H_2$  and AC. Figure 2d illustrates the schematic diagram of the ASE system driven by TiRu/Ti, wherein 0.5 M  $H_2SO_4$  catholyte and 1.0 M NaCl anolyte are separated by bipolar membrane (BPM; the cation side of BPM was directed towards the anode). The overall electrolysis performances of TiRu/Ti (+, -) in above-mentioned different systems are compared in Figure 2e. In the ASE system, it just needs a cell voltage of 1.59 V to attain  $10 \text{ mA cm}^{-2}$ , 610 and 650 mV lower than the values for SE system and diaphragm SE system, respectively, and over 50 mV lower than the ones for  $H_2SO_4 || H_2SO_4$  and  $H_2SO_4 || NaClO_4$  systems. It should be noted that different from SE system, the diaphragm just affects slightly the performance of  $H_2SO_4 || H_2SO_4$  system (Figure S14a), but has no obvious influence on its durability (Figure S14b). The energy consumption of different systems was estimated in Table S1 and presented intuitively in Figure 2f. Obviously, the ASE system requires the lowest energy input, and enables a large energy consumption decrease by 27.7% compared to direct SE system. Although the performance of TiRu/Ti (+, -) in ASE system is a little worse than that for Pt/C- $RuO_2$  at the current density below  $10 \text{ mA cm}^{-2}$ , it will surpass Pt/C- $RuO_2$  when currents exceed  $10 \text{ mA cm}^{-2}$  (Figure S15a and b). The production rate of AC at  $10 \text{ mA cm}^{-2}$  in the TiRu/Ti-based ASE system was calculated to be  $180 \mu\text{g min}^{-1} \text{ per cm}^2$ .

Meanwhile, the recorded CP curves at  $10 \text{ mA cm}^{-2}$  of different systems (Figure 2g) prove the long-term stability of the ASE system driven by TiRu/Ti (+, -). In addition, the stability test of this system at a relatively high current

density of  $50 \text{ mA cm}^{-2}$  (Figure S16a) shows that its performance has a certain decay after long-term operation due to the  $H^+$  and  $Cl^-$  consumption, pH variation and inevitable electrolyte crossover. After refreshing electrolytes, the retested CP curve is basically consistent with the initial one (Figure S16b), excluding the possibility of catalyst degradation and obvious membrane damage. The XRD (Figure S17a) and SEM (Figure S17b and c) results of TiRu/Ti in this system after over 36 h stability test at  $50 \text{ mA cm}^{-2}$  further prove its robustness. Figure S18 records the Ru 3d core-level XPS spectra of TiRu/Ti before and after HER and COR tests in this system at  $50 \text{ mA cm}^{-2}$  for over 36 h. Obviously, the Ru species in TiRu/Ti after acidic HER test is still mainly  $Ru^0$ . By contrast, the peak of Ru 3d<sub>5/2</sub> shifts to higher binding energy after COR test, indicating that there are more  $RuO_x$  species generated on the surface of TiRu/Ti. Besides, this system coupled with a 2 V photovoltaic panel under the irradiation of simulated sunlight was built (Figure 2h). When a cell voltage of  $\sim 1.59 \text{ V}$  was provided, the  $H_2$  bubbles appeared continuously on the surface of cathode (inset in Figure 2h), indicative of the high feasibility of using solar energy to actuate the ASE system.

Moreover, the feasibility of introducing natural seawater into the ASE system was studied. Figure 3a shows the image of filtered natural seawater obtained from the Yellow Sea of China. Figure 3b shows that the COR performance of TiRu/Ti in seawater is close to the one in 0.6 M NaCl, indicating that  $Cl^-$  concentration in seawater is close to 0.6 M. Therefore, we coupled 0.3 M  $H_2SO_4$  with seawater to fabricate the ASE system. Figure 3c shows the schematic diagram of the seawater-included ASE system. The performance curves

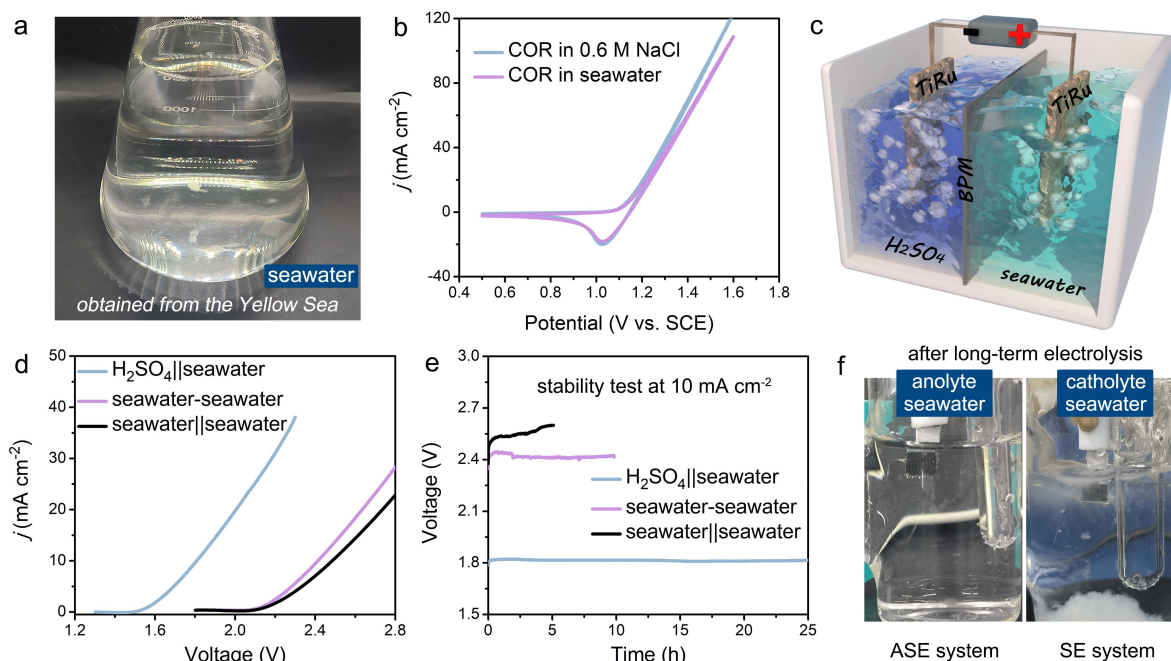


**Figure 3.** Performance evaluation of the ASE system with the introduction of natural seawater. (a) Image of natural seawater obtained from the Yellow Sea. (b) COR curves in 0.6 M NaCl and natural seawater. (c) Schematic diagram of the natural seawater-included ASE system. (d) Performance and (e) stability curves of different electrolysis systems driven by TiRu/Ti. (f) Images of anolyte seawater in the ASE system and catholyte seawater in the SE system.

(Figure 3d) of  $\text{H}_2\text{SO}_4||\text{seawater}$ , seawater-seawater (SE system) and seawater||seawater (diaphragm SE system) systems show that the seawater-included ASE system just needs a cell voltage of 1.81 V to afford  $10 \text{ mA cm}^{-2}$ , over 600 mV lower than the ones for above SE systems. Meanwhile, the stability curves (Figure 3e) of different systems at  $10 \text{ mA cm}^{-2}$  demonstrate the long-term stability of the seawater-included ASE system. Besides, we also recorded the images of anolyte seawater in the seawater-included ASE system and catholyte seawater in the SE system after long-term electrolysis (Figure 3f). Obviously, due to the acidification of anolyte seawater during electrolysis in the ASE system, the formation of Ca/Mg-based sediments is avoided, while the further alkalized catholyte seawater during electrolysis in the SE system promotes the formation of Ca/Mg-based sediments.

In order to realize real-time and controllable preparation of AEW for subsequent application, we then updated the static ASE system to the one in a half-flow mode. Figure 4a and 4b exhibit the schematic and real models of the ASE system in the half-flow mode, respectively. Movie S1 records the dynamic model of the ASE system in the half-flow mode. Figure 4c records the performances of ASE systems

in the half-flow and static modes. The almost coincident LSV curves with different concentrations of NaCl feed indicate that the half-flow mode has no obvious influence on the overall performance. The CP tests (Figure S19) of this system with different concentrations of NaCl anolyte feed further prove its operational stability for continuous preparation of AEW. The change rules of three important indicators like ACC concentration (ACC), oxidation-reduction potential (ORP) and pH for the outflowing AEW with the change of flow rate, current density and NaCl concentration were investigated (Figure 4d and Figure S20). Both ACC and ORP values decrease but pH value increases with the increase of flow rate (Figure S20a). Both ACC and ORP values increase but pH value decreases with the increase of current density (Figure S20b). Both ACC and pH values increase by different extents but ORP decreases with the increase of NaCl concentration (Figure S20c). These results could be explained by the fact that high flow rates of saline lead to insufficient anodic reactions, while higher current densities and NaCl concentrations contribute to the occurrence of anodic COR.

We attempted to explore the AEW with specific ACC as a potential sterilizer for the control of common pathogens

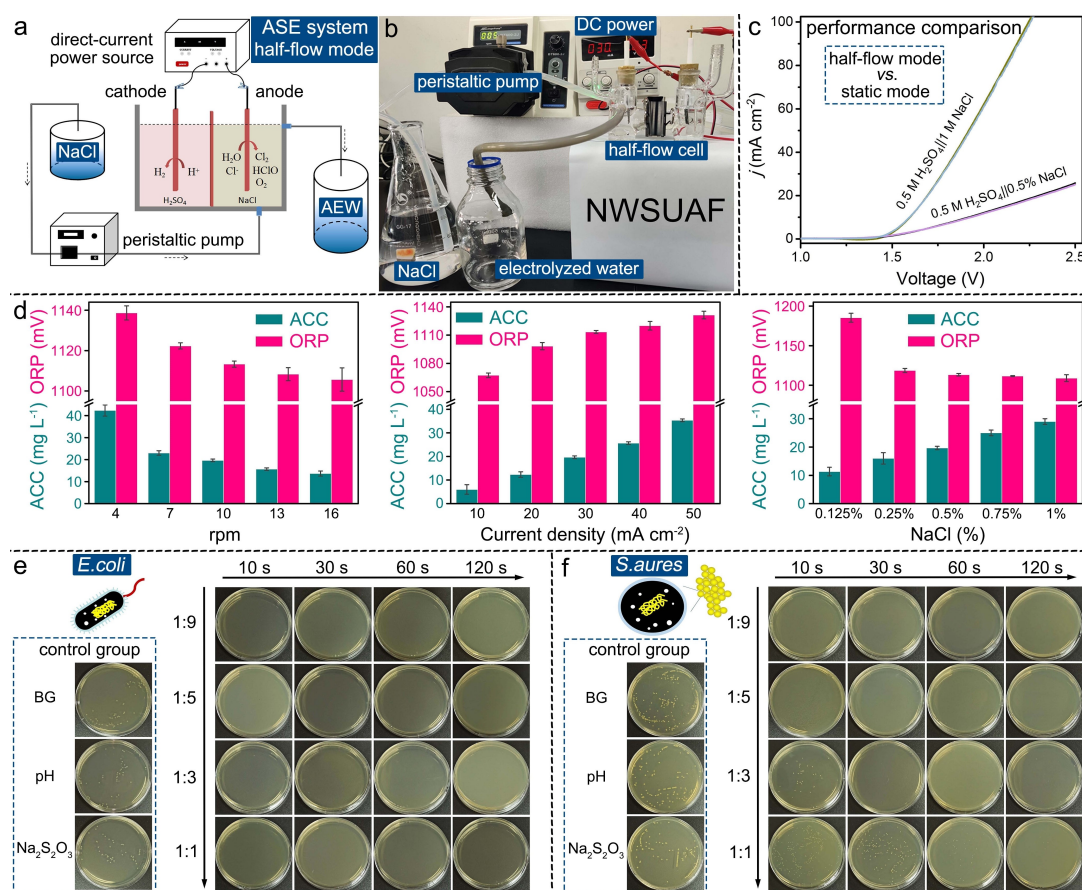


**Figure 4.** Real-time production of AC using the ASE system in the half-flow mode for sterilization. (a) Schematic and (b) real models of this system to generate  $\text{H}_2$  and AEW in real time. (c) Performance comparison of the ASE system in the static and half-flow modes with different concentrations of NaCl anolyte feed. (d) Effects of the flow rate, current density and NaCl concentration on ACC and ORP values of the prepared AEW. Sterilization efficiencies of the AEW (ACC of  $10 \text{ mg L}^{-1}$ ) toward (e) *E. coli* O157:H7 and (f) *S. aureus* with different ratios of bacterial suspension to AEW.

such as *E. coli* and *S. aureus*. As can be seen in Figure 4e, the AEW with ACC of just 10 mg L<sup>-1</sup> could inactivate rapidly the *E. coli* for 100% within just 10 s no matter for which ratio of bacterial suspension to AEW (1:9 to 1:1), whereas the pH environment and Na<sub>2</sub>S<sub>2</sub>O<sub>3</sub> terminator have no obvious effect on the disinfection of *E. coli*. For *S. aureus* (Figure 4f), when the ratio of bacterial suspension to AEW with ACC of 10 mg L<sup>-1</sup> goes below 1:5, the AEW could inactivate it rapidly for 100% within just 10 s. The SEM images of *E. coli* (Figure S21) and *S. aureus* (Figure S22) before and after treatment with AEW show that both of their surfaces become rough and wrinkled (termination within 5 min) and finally sunken (termination within 30 min). It is also worth mentioning that we did not observe obvious surface changes of *E. coli* and *S. aureus* after treatment within 30 s, meaning that surface structure damage might not be the key reason in such a short time, and the ultrafast bactericidal efficacy of AEW should be a result of joint action of multiple mechanisms.

Furthermore, the generated AEW was expected as a “green sterilizer” utilized in practical agricultural production.<sup>[14,36]</sup> Here, to inhibit the growth of natural microbiota like coliform in the production process of pea sprouts, AEW instead of water was used for pea seed soaking and sprouting. The ASE system in both the half-flow and intermittent-flow modes (Figure S23a) was ingeniously used for the generation of AEW with high ACC at low currents. To reduce the possibly existed salt stress effect, the AEW was diluted to transform into slightly AEW (SAEW) with specific ACC for watering pea seeds and sprouts (Figure S23b), and NaCl solution with the same concentration was set as control. The bactericidal effects of SAEW were determined at day 2 and 8 during seed sprouting (Figure S23c). Obviously, a higher ACC of the SAEW leads to a lower count of coliform. Specifically, compared to the control group of NaCl treatment, SAEW with ACC of 50 mg L<sup>-1</sup> could reduce the counts of coliform by 2.06 log CFU/g and 0.71 log CFU/g on the 2<sup>nd</sup> and 8<sup>th</sup> day, respectively, demonstrating the feasibility of using SAEW to reduce natural microbiota on the sprouts. The large variation of coliform counts on the 2<sup>nd</sup> and 8<sup>th</sup> days should be due to the open-ended growing environment, and the fact that the condition supplied for seed germination is also very suitable for microbe growth. Coupling SAEW with other physicochemical means might be a valid way for further improving the disinfection efficiency. The SAEW with appropriate ACC used for seed soaking and sprout spraying could also enhance the final length of pea sprouts. As shown in Figure S23d, compared with NaCl-treated group, the group treated with SAEW (ACC of 10 mg L<sup>-1</sup>) has a length enhancement of ~2 cm. This result indicates that the SAEW with suitable ACC could promote the growth of pea sprout to a certain extent.

## Conclusion

To sum up, we designed an advanced hybrid electrolysis system by coupling acidic hydrogen evolution with saline

chloride oxidation reactions. This acid-saline hybrid electrolysis system not only enables energy-saving electrosynthesis of high value-added active chlorine and H<sub>2</sub> (a large decrease of energy consumption by 27.7% compared to direct saline electrolysis system), but also promotes the generation of HClO with higher oxidation activity than ClO<sup>-</sup>. Meanwhile, the acid-seawater hybrid electrolysis system also shows largely decreased energy consumption compared with direct seawater electrolysis system, and the acidified anolyte seawater during electrolysis in this system could absolutely avoid the formation of Ca/Mg-based sediments. Besides, this system in a half-flow mode could meet the need of real-time preparation of HClO used for rapidly killing pathogens and agricultural production. Overall, this work provides a new thought for the design of advanced saline/seawater electrolysis systems used for paired electrosynthesis of active chlorine and H<sub>2</sub>.

## Acknowledgements

We thank the National Key Research and Development Program of China (No. 2023YFE0103300), the Innovative Talent Promotion Program-Science & Technology Innovation Team of Shaanxi (No. 2023-CX-TD-55), Distinguished Young Scholars (No. 52025133) and the Key Research and Development Program of Shaanxi Province (No. 2022NY-13). We thank Guoyun Zhang (State Key Laboratory of Crop Stress Biology for Arid Areas, Northwest A&F University, China) for his experimental assistance with SEM test and analysis.

## Conflict of Interest

The authors declare no conflict of interest.

## Data Availability Statement

The data that support the findings of this study are available from the corresponding author upon reasonable request.

**Keywords:** seawater electrolysis · decoupling electrolyte · active chlorine · hydrogen · energy consumption

- [1] W. Tong, M. Forster, F. Dionigi, S. Dresp, R. S. Erami, P. Strasser, A. J. Cowan, P. Farràs, *Nat. Energy* **2020**, *5*, 367–377.
- [2] Y. Liu, Y. Wang, S. Zhao, *Curr. Opin. Electrochem.* **2023**, *37*, 101202.
- [3] S. Dresp, F. Dionigi, M. Klingenhof, P. Strasser, *ACS Energy Lett.* **2019**, *4*, 933–942.
- [4] H. Ha, K. Jin, S. Park, K.-G. Lee, K. H. Cho, H. Seo, H.-Y. Ahn, Y. H. Lee, K. T. Nam, *J. Phys. Chem. Lett.* **2019**, *10*, 1226–1233.
- [5] K. S. Exner, *Phys. Chem. Chem. Phys.* **2020**, *22*, 22451–22458.
- [6] W. R. Leow, Y. Lum, A. Ozden, Y. Wang, D.-H. Nam, B. Chen, J. Wicks, T. Zhuang, F. Li, D. Sinton, E. H. Sargent, *Science* **2020**, *368*, 1228–1233.

- [7] Q. Wang, T. Li, C. Yang, M. Chen, A. Guan, L. Yang, S. Li, X. Lv, Y. Wang, G. Zheng, *Angew. Chem. Int. Ed.* **2021**, *60*, 17398–17403.
- [8] M. Chung, K. Jin, J. S. Zeng, K. Manthiram, *ACS Catal.* **2020**, *10*, 14015–14023.
- [9] S. Han, C. Cheng, M. He, R. Li, Y. Gao, Y. Yu, B. Zhang, C. Liu, *Angew. Chem. Int. Ed.* **2023**, *135*, e202216581.
- [10] L. Huang, P. Wang, Y. Jiang, K. Davey, Y. Zheng, S.-Z. Qiao, *J. Am. Chem. Soc.* **2023**, *145*, 15565–15571.
- [11] Y. Wang, Y. Xue, C. Zhang, *Small* **2021**, *17*, 2006587.
- [12] L. Su, D. Han, G. Zhu, H. Xu, W. Luo, L. Wang, W. Jiang, A. Dong, J. Yang, *Nano Lett.* **2019**, *19*, 5423–5430.
- [13] Y. Chen, G. Zhang, Q. Ji, H. Lan, H. Liu, J. Qu, *Environ. Sci. Technol.* **2022**, *56*, 9722–9731.
- [14] S. Rahman, I. Khan, D.-H. Oh, *Compr. Rev. Food Sci. Food Saf.* **2016**, *15*, 471–490.
- [15] Y. Takeda, H. Uchiumi, S. Matsuda, H. Ogawa, *Biochem. Bioph. Res. Co.* **2020**, *530*, 1–3.
- [16] C. Zhang, G. Yang, P. Shen, Y. Shi, Y. Yang, Y. Liu, X. Xia, S. Wang, *Food Microbiol.* **2022**, *103*, 103951.
- [17] N.-N. Liang, D. S. Han, H. Park, *Appl. Catal. B* **2023**, *324*, 122275.
- [18] Y. Wang, Y. Liu, D. Wiley, S. Zhao, Z. Tang, *J. Mater. Chem. A* **2021**, *9*, 18974–18993.
- [19] N. Wang, P. Ou, S.-F. Hung, J. E. Huang, A. Ozden, J. Abed, I. Grigioni, C. Chen, R. K. Miao, Y. Yan, J. Zhang, Z. Wang, R. Dorakhan, A. Badreldin, A. Abdel-Wahab, D. Sinton, Y. Liu, H. Liang, E. H. Sargent, *Adv. Mater.* **2023**, *35*, 2210057.
- [20] J. Yang, W.-H. Li, K. Xu, S. Tan, D. Wang, Y. Li, *Angew. Chem. Int. Ed.* **2022**, *134*, e202200366.
- [21] T. Lim, G. Y. Jung, J. H. Kim, S. O. Park, J. Park, Y.-T. Kim, S. J. Kang, H. Y. Jeong, S. K. Kwak, S. H. Joo, *Nat. Commun.* **2020**, *11*, 412.
- [22] Y. Yao, L. Zhao, J. Dai, J. Wang, C. Fang, G. Zhan, Q. Zheng, W. Hou, L. Zhang, *Angew. Chem. Int. Ed.* **2022**, *61*, e202208215.
- [23] Y. Liu, C. Li, C. Tan, Z. Pei, T. Yang, S. Zhang, Q. Huang, Y. Wang, Z. Zhou, X. Liao, J. Dong, H. Tan, W. Yan, H. Yin, Z.-Q. Liu, J. Huang, S. Zhao, *Nat. Commun.* **2023**, *14*, 2475.
- [24] J. Yang, W. Li, H. Tang, Y. Pan, D. Wang, Y. Li, *Nature* **2023**, *617*, 519–523.
- [25] H. W. Lim, D. K. Cho, J. H. Park, S. G. Ji, Y. J. Ahn, J. Y. Kim, C. W. Lee, *ACS Catal.* **2021**, *11*, 12423–12432.
- [26] T. Ni, H. Feng, J. Tang, J. Wang, J. Yu, Y. Yi, Y. Wu, Y. Guo, L. Tang, *Chemosphere* **2022**, *300*, 134449.
- [27] J. Guo, Y. Zheng, Z. Hu, C. Zheng, J. Mao, K. Du, M. Jaroniec, S.-Z. Qiao, T. Ling, *Nat. Energy* **2023**, *8*, 264–272.
- [28] L. Wu, L. Yu, B. McElhenny, X. Xing, D. Luo, F. Zhang, J. Bao, S. Chen, Z. Ren, *Appl. Catal. B* **2021**, *294*, 120256.
- [29] B. Zheng, L. Ma, B. Li, D. Chen, X. Li, J. He, J. Xie, M. Robert, T. Lau, *Catal. Sci. Technol.* **2020**, *10*, 4405–4411.
- [30] Y. Feng, S. Lu, L. Fu, F. Yang, L. Feng, *Chem. Sci.* **2024**, *15*, 2123–2132.
- [31] J. Jiang, W. Wei, Z. Ren, Y. Luo, X. Wang, Y. Xu, M. Chang, L. Ai, *J. Colloid Interface Sci.* **2023**, *646*, 25–33.
- [32] S. Nong, W. Dong, J. Yin, B. Dong, Y. Lu, X. Yuan, X. Wang, K. Bu, M. Chen, S. Jiang, L. Liu, M. Sui, F. Huang, *J. Am. Chem. Soc.* **2018**, *140*, 5719–5727.
- [33] A. Sinhamahapatra, J.-P. Jeon, J.-S. Yu, *Energy Environ. Sci.* **2015**, *8*, 3539–3544.
- [34] S. A. Abdullah, M. Z. Sahdan, N. Nayan, Z. Embong, C. R. C. Hak, F. Adriyanto, *Mater. Lett.* **2020**, *263*, 127143.
- [35] L. Wu, L. Yu, F. Zhang, B. McElhenny, D. Luo, A. Karim, S. Chen, Z. Ren, *Adv. Funct. Mater.* **2021**, *31*, 2006484.
- [36] W. Zhang, J. Cao, W. Jiang, *Trends Food Sci. Tech.* **2021**, *114*, 599–607.

Manuscript received: December 21, 2023

Accepted manuscript online: February 14, 2024

Version of record online: ■■■, ■■■

## Research Articles

## Seawater Electrolysis

W. Zhu, Z. Wei, Y. Ma, M. Ren, X. Fu, M. Li,  
C. Zhang, J. Wang,\*  
S. Guo\* \_\_\_\_\_ e202319798

Energy-Efficient Electrosynthesis of High Value-Added Active Chlorine Coupled with H<sub>2</sub> Generation from Direct Seawater Electrolysis through Decoupling Electrolytes



An acid-saline hybrid electrolysis system is developed for energy-saving electro-synthesis of HClO and H<sub>2</sub>. This system requires a low cell voltage of 1.59 V to attain 10 mA cm<sup>-2</sup> with a large energy consumption decrease of 27.7% compared with direct saline electrolysis system (2.20 V).